

The Iteratively Regularized Gauß-Newton Method with Convex Constraints and Applications in 4Pi-Microscopy

Robert Stück, Martin Burger and Thorsten Hohage

Abstract

This paper is concerned with the numerical solution of nonlinear ill-posed operator equations involving convex constraints. We study a Newton-type method which consists in applying linear Tikhonov regularization with convex constraints to the Newton equations in each iteration step. Convergence of this iterative regularization method is analyzed if both the operator and the right hand side are given with errors and all error levels tend to zero. Our study has been motivated by the joint estimation of object and phase in 4Pi microscopy, which leads to a semi-blind deconvolution problem with nonnegativity constraints. The performance of the proposed algorithm is illustrated both for simulated and for three-dimensional experimental data.

1 Introduction

In this paper we present and analyze a Newton-type regularization method for nonlinear ill-posed operator equations with convex constraints. More specifically, let \mathcal{X} and \mathcal{Y} be Hilbert spaces, $\mathcal{C} \subset \mathcal{X}$ a nonempty, closed convex set, and $F : \mathcal{C} \rightarrow \mathcal{Y}$ a “forward” operator, which we assume to be Gateaux differentiable. We consider the inverse problem of reconstructing x^\dagger in the operator equation

$$F(x^\dagger) = g, \quad x^\dagger \in \mathcal{C} \tag{1.1}$$

if only noisy versions of both F and g are given. Moreover, we aim to prove convergence of such reconstructions as the noise levels tend to zero.

An inverse problem for which it is particularly important to properly incorporate a convex constraint into the inversion scheme arises in a confocal fluorescence microscopy technique (cf. [17]) called 4Pi microscopy. This technique was suggested and developed by Hell et.al. [9, 10] and allows for a substantial enhancement of resolution using interference of two laser beams in the microscopic focus and/or interference of fluorescence photons on the detector. In standard confocal microscopy the relation between the unknown fluorescent marker density

$f \in L^2(\mathbb{R}^3)$ of the specimen and the measured intensity g is given by a convolution with a *point spread function* (psf) $h \in L^1(\mathbb{R}^3)$, which is often modeled as a Gaussian function:

$$g(\mathbf{x}) = \int h(\mathbf{x} - \mathbf{y})f(\mathbf{y}) d\mathbf{y} \quad (1.2)$$

The width of h is typically much larger along the so-called optical axis (which we assume to be the x_3 -axis) than in directions perpendicular to the optical axis.

4Pi microscopy allows an increase of resolution along the optical axis by a factor of 3–7 using interference of coherent photons through two opposing objective lenses. Here the psf is no longer spatially invariant in general, but depends on the relative phase $\phi(\mathbf{x})$ of the interfering photons, which has to be recovered together with the fluorophore density f in general since it depends on the refractive index of the specimen which is unknown. The imaging process can be modeled by an operator equation $F_{4\text{Pi}}(f, \phi) = g$ with a forward operator of the form

$$F_{4\text{Pi}}(f, \phi)(\mathbf{x}) := \int p(\mathbf{y} - \mathbf{x}, \phi(\mathbf{x}))f(\mathbf{y})d\mathbf{y}. \quad (1.3)$$

Note that F is nonlinear in ϕ and that $f \mapsto F(f, \phi)$ is not a convolution operator in general. As a density, f has to be nonnegative. Therefore, we have the convex constraint $(f, \phi) \in \mathcal{C}$ with $\mathcal{C} := \{(f, \phi) : f \geq 0\}$. A simple frequently used model for the 4Pi-psf (cf., e.g., [1]) is given by

$$p(\mathbf{x}, \varphi) \approx h(\mathbf{x}) \cos^n \left(cx_3 + \frac{\varphi}{2} \right), \quad (1.4)$$

where h is the psf of the corresponding confocal microscope, and the cosine term represents the interference pattern for different types of 4Pi-microscopes corresponding to $n = 2, 4$, respectively (see Fig. 1.1). So far reconstruction of f in commercially available 4Pi microscopes is done by standard deconvolution software assuming the relative phase function ϕ to be constant. Although spatial variations of ϕ can approximately be avoided experimentally in some situations, the assumption that ϕ is constant imposes severe limitations on the applicability and reliability of 4Pi microscopy. Therefore, it is of great interest to develop algorithms for the solution of the convexly constrained nonlinear inverse problem to recover both the object function f and the relative phase function ϕ from the data g .

To this end we propose and analyze the following constrained version of the iteratively regularized Gauß-Newton method (IRGNM). We assume that both the right hand side g in the operator equation (1.1) and the operator F are only given approximately with errors by g_δ and F_δ , respectively. Error bounds will be specified in the next section. Given some initial guess $x_0 \in \mathcal{C}$, we consider the iteration

$$x_{n+1} = \underset{x \in \mathcal{C}}{\operatorname{argmin}} \left[\|F'_\delta[x_n](x - x_n) + F_\delta(x_n) - g_\delta\|^2 + \alpha_n \|x - x_0\|^2 \right], \quad (1.5a)$$

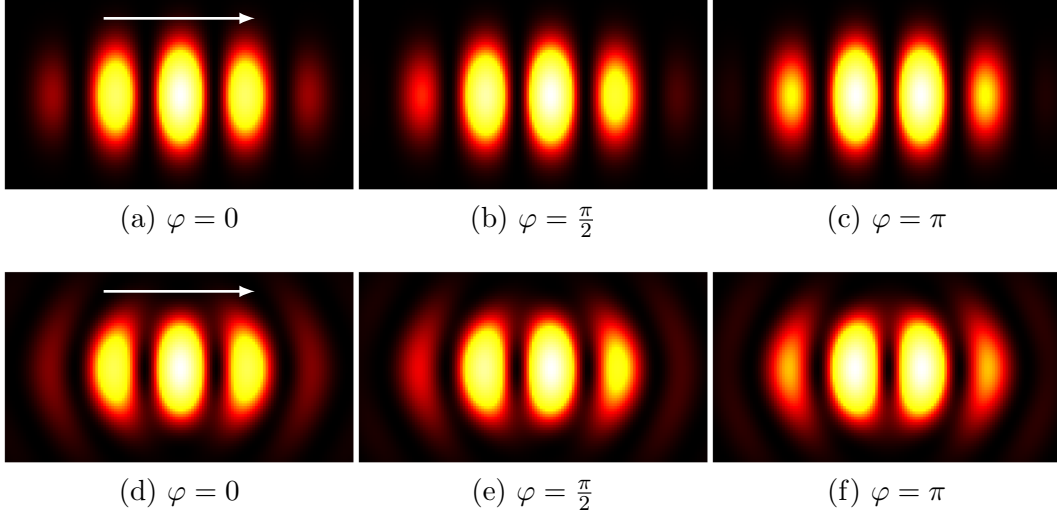


Figure 1.1: The top line shows the psf of a 4Pi microscope modeled by (1.4) for relative phases $\varphi = 0, \frac{\pi}{2}, \pi$ on the plane containing the optical axis, which is indicated by the white arrow. The bottom line shows the more accurate model (3.1).

$n = 0, 1, 2, \dots$, with a sequence of regularization parameters α_n satisfying

$$1 \leq \frac{\alpha_n}{\alpha_{n+1}} \leq r, \quad \lim_{n \rightarrow \infty} \alpha_n = 0, \quad \alpha_n > 0 \quad \text{for some } r > 1 \text{ and for all } n \in \mathbb{N}_0. \quad (1.5b)$$

In the unconstrained case $\mathcal{C} = \mathcal{X}$ this reduces to the IRGNM as suggested in the original paper by Bakushinskiĭ [2]. For $\mathcal{C} \neq \mathcal{X}$ a quadratic minimization problem with convex constraint has to be solved in each Newton step. In [2] convergence rates were shown for Hölder type source conditions with exponent $\nu = 1$. In [4, 12] order optimal convergence rates for more general Hölder type and logarithmic source conditions were proven. For numerous further references on the IRGNM and other iterative regularization methods we refer to the monographs [3, 15]. More recently, Kaltenbacher and Hofmann [14] proved optimal convergence rates of the IRGNM in Banach spaces for general source conditions.

The convergence result we will present in the next section (Theorem 2.1) takes into account two features, which are essential for 4Pi reconstructions and are not covered in the literature so far: First of all, our source condition takes into account the convex constraint and is weaker than the corresponding source condition for the unconstrained case, yielding the same rate of convergence. This reflects the observation reported below that projecting reconstructions of the unconstrained IRGNM onto \mathcal{C} does not yield competitive results. For linear Tikhonov regularization with convex constraints we refer to Neubauer [16] and [6, section 5.4]. Moreover, unlike many other references on the IRGNM, we also take into account errors in the operator since they are important in our application: The frequently used model (1.4) for the 4Pi psf is only a first approximation, and

even the more accurate model based on the evaluation of diffraction integrals, which we used in our code (see Fig. 1.1 and eq. (3.1) below), contains parameters, which have to be estimated including errors. Other references discussing the influence of errors in the operator for the IRGNM include [3] and [13].

The plan of this paper is as follows: Our main convergence result, Theorem 2.1, is formulated and proved in Section 2. Section 3 contains a more detailed discussion of 4Pi microscopy and the model (1.3), a comparison with other methods, and numerical results both for simulated and experimental data.

2 IRGNM with Convex Constraints

2.1 Formulation of the theorem

We assume that $F, F_\delta : \mathcal{C} \rightarrow \mathcal{Y}$ are both Gateaux differentiable with bounded derivatives $F'[x], F'_\delta[x]$ for all $x \in \mathcal{C}$ and that the following error bounds hold:

$$\|g - g_\delta\| \leq \delta_g, \quad (2.1a)$$

$$\left\| F(x^\dagger) - F_\delta(x^\dagger) \right\| \leq \delta_F \quad (2.1b)$$

$$\left\| F'[x^\dagger] - F'_\delta[x^\dagger] \right\| \leq \delta_{F'} \quad (2.1c)$$

with noise levels $\delta_g, \delta_F, \delta_{F'} \geq 0$.

Further we assume that a source condition of the form

$$x^\dagger = P_{\mathcal{C}}(F'[x^\dagger]^* \omega + x_0) \quad \text{for some } \omega \in \mathcal{Y} \text{ with } \|\omega\| \leq \rho \quad (2.2a)$$

is satisfied where $P_{\mathcal{C}} : \mathcal{X} \rightarrow \mathcal{C}$ denotes the metric projection onto \mathcal{C} . The source condition (2.2a) corresponds to the one for linear constrained Tikhonov regularization we assume in Lemma 2.2, and since $\mathcal{R}(T^*) = \mathcal{R}((T^*T)^{1/2})$ for a bounded linear operator $T : \mathcal{X} \rightarrow \mathcal{Y}$ (cf. [6, Proposition 2.18]) it corresponds to a Hölder-type source condition with exponent $\nu = \frac{1}{2}$. As the (2.2a) contains the projector $P_{\mathcal{C}}$, it is less restrictive than in the unconstrained case $\mathcal{C} = \mathcal{X}$. In particular, x^\dagger may not be smooth even if $F'[x^\dagger]^*$ is smoothing and x_0 is smooth.

If $F'[x^\dagger]$ is not injective, we further assume that x^\dagger satisfies

$$x^\dagger = \underset{\{x \in \mathcal{C} : F'[x^\dagger](x - x^\dagger) = 0\}}{\operatorname{argmin}} \|x - x_0\|. \quad (2.2b)$$

Obviously, this condition is empty if $F'[x^\dagger]$ is injective. Moreover, if for any $v_0 \in N(F'[x^\dagger])$ there exists a differentiable curve $v : [0, \epsilon) \rightarrow \mathcal{C}$ with $v(0) = x^\dagger$, $v'(0) = v_0$ and $F(v(t)) = g$ for all t (see e.g. [8] for a problem where this condition is satisfied), then it is easy to see that (2.2b) follows from $x^\dagger = \operatorname{argmin}_{\{x \in \mathcal{C} : F(x) = g\}} \|x - x_0\|$.

As nonlinearity condition on the operator F_δ we only need to assume that for some $\gamma > 0$ there exists a Lipschitz constant $L > 0$ such that

$$\left\| F'_\delta[x] - F'_\delta[x^\dagger] \right\| \leq L \left\| x - x^\dagger \right\| \quad \text{for all } x \in \mathcal{C} \text{ with } \left\| x - x^\dagger \right\| \leq \gamma. \quad (2.3)$$

We can now formulate our main convergence theorem:

Theorem 2.1. *Assume that (1.1) and (2.1)–(2.3) are satisfied with ρ is sufficiently small, set*

$$\bar{\delta} := \max(\delta_g + \delta_F, \delta_{F'}^2), \quad (2.4)$$

and consider the sequence (x_n) defined by (1.5).

Then the iterates satisfy $\|x_n - x^\dagger\| \leq \gamma$ and in the noise free case $\bar{\delta} = 0$ we have

$$\|x_n - x^\dagger\| = \mathcal{O}(\sqrt{\alpha_n}), \quad n \rightarrow \infty. \quad (2.5)$$

For $\bar{\delta} > 0$ assume that a stopping index N is chosen such that

$$\alpha_N < \eta \bar{\delta} \leq \alpha_n, \quad 0 \leq n < N \quad (2.6)$$

with some constant $\eta > 0$ sufficiently large. Then the error of the final approximation fulfills

$$\|x_N - x^\dagger\| = \mathcal{O}(\sqrt{\bar{\delta}}), \quad \bar{\delta} \rightarrow 0. \quad (2.7)$$

2.2 Proof of the theorem

Note that if $F = F_\delta = T : \mathcal{X} \rightarrow \mathcal{Y}$ is linear and bounded, then (1.5a) reduces to linear constrained Tikhonov regularization

$$x_\alpha := \operatorname{argmin}_{x \in \mathcal{C}} \left[\|Tx - g_\delta\|^2 + \alpha \|x - x_0\|^2 \right] \quad (2.8)$$

for a sequence of regularization parameter $\alpha = \alpha_n$. We first recall the stability and approximation properties in this case since they will be needed later in the proof.

Lemma 2.2. *1. If*

$$\bar{x}_\alpha := \operatorname{argmin}_{x \in \mathcal{C}} \left[\|Tx - \bar{g}_\delta\|^2 + \alpha \|x - x_0\|^2 \right]$$

for some $\bar{g}_\delta \in \mathcal{Y}$, then

$$\|x_\alpha - \bar{x}_\alpha\| \leq \frac{\|g_\delta - \bar{g}_\delta\|}{\alpha}. \quad (2.9)$$

2. Let $g = g^\delta \in T(\mathcal{C})$ and $x_0 \in \mathcal{C}$, and assume that the best-approximate-solution $x_\mathcal{C}^\dagger := \operatorname{argmin}_{\{x \in \mathcal{C}: Tx=g\}} \|x - x_0\|$ satisfies the source condition

$$x_\mathcal{C}^\dagger = P_\mathcal{C}(T^*\omega + x_0) \quad (2.10)$$

for some $\omega \in \mathcal{Y}$. Then

$$\|x_\alpha - x_\mathcal{C}^\dagger\| = \sqrt{\alpha} \|\omega\| \quad \text{and} \quad \|Tx_\alpha - g\| = \alpha \|\omega\|. \quad (2.11)$$

Proof. In (2.9) the special case $x_0 = 0$ is proved in [6, Theorem 5.16]. The general case can be reduced to this special case by the substitution of variables $z = x - x_0$ since

$$x_\alpha - x_0 = \operatorname{argmin}_{z \in \mathcal{C} - x_0} \left[\|Tz + Tx_0 - g_\delta\|^2 + \alpha \|z\|^2 \right]. \quad (2.12)$$

(2.11) can be reduced to the case $x_0 = 0$, which is covered by [6, Theorem 5.19], by the same substitution of variables and the identity $P_{\mathcal{C} - x_0}(T^*\omega) = P_{\mathcal{C}}(T^*\omega + x_0) - x_0$. \square

Next we need a stability estimate with respect to perturbations of the operators, i.e. an estimate on the difference of

$$x_i := \operatorname{argmin}_{x \in \mathcal{C}} \left[\|T_i(x - \tilde{x})\|^2 + \alpha \|x - x_0\|^2 \right], \quad i \in \{1, 2\}, \quad (2.13)$$

where $T_1, T_2 : \mathcal{X} \rightarrow \mathcal{Y}$ are bounded linear operators and $\alpha > 0$. Using the optimality conditions for the minimizers of (2.13), a straightforward computation gives an estimate of the form

$$\|x_1 - x_2\| \leq \frac{c}{\alpha} \|T_1 - T_2\|. \quad (2.14)$$

This simple estimate is not sufficient for our purposes, however. The following proposition shows that under a source condition we can obtain an improved estimate with a constant independent of α :

Proposition 2.3. *Let x_1 and x_2 be defined by (2.13). Moreover, let the source condition*

$$\tilde{x} = P_{\mathcal{C}}(T_2^*\omega + x_0) \quad (2.15)$$

hold for some $\omega \in \mathcal{Y}$ and let $\tilde{x} = \operatorname{argmin}_{\{x \in \mathcal{C} : T_2x = T_2\tilde{x}\}} \|x - x_0\|$. Then the distance of x_1 and x_2 is bounded by

$$\|x_1 - x_2\| \leq \sqrt{\frac{3}{2}} \|\omega\| \|T_1 - T_2\|.$$

Proof. From Lemma 2.2, part 2 we obtain

$$\|T_2(x_2 - \tilde{x})\| \leq \alpha \|\omega\| \quad (2.16a)$$

$$\|x_2 - \tilde{x}\| \leq \sqrt{\alpha} \|\omega\|. \quad (2.16b)$$

Let $\chi_{\mathcal{C}} : X \rightarrow \mathbb{R}^+$ be the proper, convex and lower semicontinuous functional

$$\chi_{\mathcal{C}}(x) := \begin{cases} 0 & x \in \mathcal{C} \\ \infty & \text{otherwise} \end{cases},$$

and let $q_i \in \partial\chi_{\mathcal{C}}(x_i)$, then for $i \in \{1, 2\}$ the first order optimality condition for the minimizers x_i is given by

$$T_i^*T_i(x_i - \tilde{x}) + \alpha(x_i - x_0) + q_i = 0. \quad (2.17)$$

Subtracting the equations (2.17) gives

$$T_1^* T_1(x_1 - x_2) + \alpha(x_1 - x_2) + (q_1 - q_2) = (T_2^* T_2 - T_1^* T_1)(x_2 - \tilde{x}).$$

Now taking the inner product with $x_1 - x_2$ we obtain

$$\begin{aligned} & \|T_1(x_1 - x_2)\|^2 + \alpha \|x_1 - x_2\|^2 + \langle q_1 - q_2, x_1 - x_2 \rangle = \\ & \langle (T_2^* - T_1^*) T_2(x_2 - \tilde{x}), x_1 - x_2 \rangle + \langle (T_2 - T_1)(x_2 - \tilde{x}), T_1(x_1 - x_2) \rangle. \end{aligned} \quad (2.18)$$

The right hand side can be estimated with help of Young's inequality

$$\begin{aligned} & \langle (T_2^* - T_1^*) T_2(x_2 - \tilde{x}), x_1 - x_2 \rangle + \langle (T_2 - T_1)(x_2 - \tilde{x}), T_1(x_1 - x_2) \rangle \\ & \leq \frac{1}{2\alpha} \|T_1 - T_2\|^2 \|T_2(x_2 - \tilde{x})\|^2 + \frac{\alpha}{2} \|x_1 - x_2\|^2 + \frac{1}{4} \|T_1 - T_2\|^2 \|x_2 - \tilde{x}\|^2 + \|T_1(x_1 - x_2)\|^2. \end{aligned} \quad (2.19)$$

Using $\langle q_1 - q_2, x_1 - x_2 \rangle \geq 0$ (see, e.g., [7, Section 9.6.1, Theorem 1]), (2.19) and the inequalities (2.16) the assertion follows from

$$\begin{aligned} \frac{\alpha}{2} \|x_1 - x_2\|^2 & \leq \frac{1}{2\alpha} \|T_2(x_2 - \tilde{x})\|^2 \|T_1 - T_2\|^2 + \frac{1}{4} \|x_2 - \tilde{x}\|^2 \|T_1 - T_2\|^2 \\ & \leq \frac{3}{4} \alpha \|\omega\|^2 \|T_1 - T_2\|^2. \end{aligned}$$

□

Now we are able to formulate a recursive error estimate for the IRGNM with closed convex constraint.

Lemma 2.4. *Assume that (1.1) and (1.5)–(2.3) are satisfied and that $x_n \in \mathcal{C}$ with $\|x_n - x^\dagger\| \leq \gamma$, then the error $e_n := x_n - x^\dagger$ satisfies*

$$\|e_{n+1}\| \leq \frac{1}{\sqrt{\alpha_n}} \frac{L}{2} \|e_n\|^2 + \sqrt{\frac{3}{2}} \rho L \|e_n\| + \frac{1}{\sqrt{\alpha_n}} (\delta_g + \delta_F) + \sqrt{\alpha_n} \rho + \sqrt{\frac{3}{2}} \rho \delta_{F'}. \quad (2.20)$$

Proof. At first we note that one can express the noisy data as $g_\delta = F_\delta(x^\dagger) + \xi + \epsilon$, with $\|\xi\| \leq \delta_F$ and $\|\epsilon\| \leq \delta_g$. Further since $x_n \in \mathcal{C}$ and F_δ is Gateaux differentiable with derivatives that fulfill condition (2.3), we can express $F_\delta(x^\dagger)$ in a Taylor series

$$F_\delta(x^\dagger) = F_\delta(x_n) + F'_\delta[x_n](x^\dagger - x_n) + r(x^\dagger - x_n), \quad (2.21)$$

where

$$\|r(x^\dagger - x_n)\| \leq \frac{L}{2} \|x^\dagger - x_n\|^2. \quad (2.22)$$

Thus we can rewrite the IRGNM functional (1.5a) of the n -th iteration step, defining $T_n := F'_\delta[x_n]$, as

$$\|T_n x - (T_n x_n - F_\delta(x_n) + g_\delta)\|^2 + \alpha_n \|x - x_0\|^2 \quad (2.23)$$

$$= \left\| T_n(x - x^\dagger) - r(x^\dagger - x_n) - \xi - \epsilon \right\|^2 + \alpha_n \|x - x_0\|^2. \quad (2.24)$$

Now we can decompose the distance of the solution x_{n+1} of the $(n+1)$ -th iteration to the exact solution x^\dagger using the triangle inequality

$$\|x_{n+1} - x^\dagger\| \leq \|x_{n+1} - x_{\alpha_n, n}\| + \|x_{\alpha_n, n} - x_{\alpha_n}\| + \|x_{\alpha_n} - x^\dagger\| \quad (2.25)$$

with

$$\begin{aligned} x_{n+1} &= \operatorname{argmin}_{x \in \mathcal{C}} \left[\|T_n(x - x^\dagger) - r_n(x^\dagger - x_n) - \xi - \epsilon\|^2 + \alpha_n \|x - x_0\|^2 \right] \\ x_{\alpha_n, n} &:= \operatorname{argmin}_{x \in \mathcal{C}} \left[\|T_n(x - x^\dagger)\|^2 + \alpha_n \|x - x_0\|^2 \right] \\ x_{\alpha_n} &:= \operatorname{argmin}_{x \in \mathcal{C}} \left[\|F'[x^\dagger](x - x^\dagger)\|^2 + \alpha_n \|x - x_0\|^2 \right]. \end{aligned}$$

It follows from Lemma 2.2, part 1 that

$$\|x_{n+1} - x_{\alpha_n, n}\| \leq \frac{\|r_n(x^\dagger - x_n) + \xi + \epsilon\|}{\sqrt{\alpha_n}}. \quad (2.27)$$

With (2.22), $\|\xi\| \leq \delta_F$ and $\|\epsilon\| \leq \delta_g$ we obtain

$$\|x_{n+1} - x_{\alpha_n, n}\| \leq \frac{1}{\sqrt{\alpha_n}} \left(\frac{L}{2} \|x_n - x^\dagger\|^2 + \delta_F + \delta_g \right). \quad (2.28)$$

The second term in (2.25) can be estimated using Proposition 2.3 with $T_1 = T_n$, $T_2 = F'[x^\dagger]$ and $\tilde{x} = x^\dagger$, which gives

$$\begin{aligned} \|x_{\alpha_n, n} - x_{\alpha_n}\| &\leq \sqrt{\frac{3}{2}} \rho \|T_n - F'[x^\dagger]\| \\ &\leq \sqrt{\frac{3}{2}} \rho \left(\|T_n - F'_\delta[x^\dagger]\| + \|F'_\delta[x^\dagger] - F'[x^\dagger]\| \right) \\ &\leq \sqrt{\frac{3}{2}} \rho \left(L \|x_n - x^\dagger\| + \delta_{F'} \right), \end{aligned} \quad (2.29)$$

where we used (2.3) and (2.1c) to obtain the last inequality of (2.29). For the third term in (2.25) we again use Lemma 2.2, part 2 to obtain

$$\|x_{\alpha_n} - x^\dagger\| \leq \sqrt{\alpha_n} \rho. \quad (2.30)$$

Combining (2.25), (2.28), (2.29) and (2.30) gives the assertion. \square

Estimate (2.20) is of the form used in [4] and [12], so we can use a similar proof now to obtain the main result.

Proof of Theorem 2.1. It follows from Lemma 2.4 that the quantities $\Theta_n := \frac{\|e_n\|}{\sqrt{\alpha_n}}$ fulfill the inequality

$$\Theta_{n+1} \leq a + b\Theta_n + c\Theta_n^2 \quad (2.31)$$

with $a := \sqrt{r}\rho$ for $\bar{\delta} = 0$ and $a := \sqrt{r}(\rho + \frac{\delta_a + \delta_F}{\eta\bar{\delta}} + \sqrt{\frac{3}{2}}\rho\frac{\delta_{F'}}{\sqrt{\eta\bar{\delta}}})$ for $\bar{\delta} > 0$, $b := \sqrt{\frac{3}{2}}r\rho L$ and $c := \sqrt{r}\frac{L}{2}$. Let t_1 and t_2 be solutions to the fixed point equation $a+bt+ct^2 = t$, i.e.

$$t_1 := \frac{2a}{1-b+\sqrt{(1-b)^2-4ac}} \quad t_2 := \frac{1-b+\sqrt{(1-b)^2-4ac}}{2c}, \quad (2.32)$$

let the stopping index $N \leq \infty$ be given by (2.6) and define $C_\Theta := \max(\Theta_0, t_1)$. We will show by induction that

$$\Theta_n \leq C_\Theta \quad (2.33)$$

for $0 \leq n \leq N$ if

$$b + 2\sqrt{ac} < 1, \quad (2.34a)$$

$$\Theta_0 \leq t_2, \quad (2.34b)$$

$$\sqrt{\alpha_0}C_\Theta \leq \gamma. \quad (2.34c)$$

Conditions (2.34) are satisfied if ρ is sufficiently small and η sufficiently large. For $n = 0$ (2.33) is true by the definition of C_Θ . Assume that (2.33) is true for some $k < N$, then by (2.34c) and Lemma 2.4, (2.31) is true for $n = k$. Condition (2.34a) assures that $t_1, t_2 \in \mathbb{R}$ and $t_1 < t_2$, and by (2.33) one has $0 \leq \Theta_k \leq t_1$ or $t_1 \leq \Theta_k \leq \Theta_0$. In the first case, since $a, b, c \geq 0$, we obtain

$$\Theta_{k+1} \leq a + b\Theta_k + c\Theta_k^2 \leq a + bt_1 + ct_1^2 = t_1. \quad (2.35)$$

In the second case by (2.34b) and the fact that $a + (b-1)t + ct^2 \leq 0$ for $t_1 \leq t \leq t_2$ we obtain

$$\Theta_{k+1} \leq a + b\Theta_k + c\Theta_k^2 \leq \Theta_k \leq \Theta_0. \quad (2.36)$$

Thus in both cases (2.33) holds for $n = k + 1$ and the induction is complete.

By definition $N = \infty$ for $\bar{\delta} = 0$ and thus (2.33) directly implies (2.5). Using $\alpha_N < \eta\bar{\delta}$ by (2.6) also assertion (2.7) follows directly from (2.33). \square

3 Joint reconstruction of object and phase in 4Pi-microscopy

Before we describe our mathematical model of the 4Pi imaging process precisely, let us discuss this technique in some more detail. Confocal fluorescence microscopy allows the reconstruction of three-dimensional fluorescent marker densities in living cells by scanning a specimen at a grid of points $\{\mathbf{x}_j \in \mathbb{R}^3 : j = 1, \dots, N\}$. Laser light is focused to a small area by objective lenses, and a pinhole is used to collect only fluorescence photons emitted close to the focus \mathbf{x}_j (cf. [17]). The psf $h(\mathbf{x} - \mathbf{y})$ in (1.2) is the probability that a fluorescence photon emitted

at \mathbf{y} is detected if the point \mathbf{x} is illuminated. Data consist of photon count numbers G_j , $j = 1, \dots, N$, which are Poisson distributed random numbers with mean $\mathbf{E}G_j = g(\mathbf{x}_j)$.

In 4Pi microscopy the same data model holds true, but g is given by $g = F_{4\text{Pi}}(f, \phi)$ with the integral operator (1.3). For its kernel we use the more accurate model

$$p(\mathbf{z}, \varphi) = |\mathbf{E}_1(z) - \exp(i\phi)\mathbf{E}_2(z)|^2 h_{\text{det}}(\mathbf{z}) \quad (3.1)$$

(see [18]) instead of the simple model (1.4). Here $\mathbf{E}_{1,2}$ are counterpropagating focal fields and h_{det} is the detection psf, for which we used implementations available under www.imspector.de.

3.1 forward operator and its derivative

We first define appropriate function spaces for the integral operator $F_{4\text{Pi}}$ in (1.3). We assume that f is supported in some cube $\Omega := \prod_{j=1}^3 [-R_j, R_j]$ and choose $L^2(\Omega)$ with the standard L^2 -norm as function space for the object f . We may further assume that $p(\cdot, \varphi)$ is supported in some (typically much smaller) cube $\prod_{j=1}^3 [-r_j, r_j]$ for all φ such that g is supported in $\Omega' := \prod_{j=1}^3 [-R_j - r_j, R_j + r_j]$.

A reason why joint reconstruction of f and ϕ from data g often works even though the problem is formally underdetermined, is that ϕ can be assumed to be very smooth (often it is even assumed to be constant). Therefore we choose the Sobolev space $H^2(\Omega')$ for ϕ with norm $\|\phi\|_{H^2(\Omega')} := (\int_{\Omega'} |\phi|^2 + |\nabla\phi|^2 + |\Delta\phi|^2 dx)^{\frac{1}{2}}$ to achieve smooth interpolation in areas where no information on ϕ is contained in the data. (This is the case, e.g., in areas where f is constant. But in such areas ϕ is irrelevant for the primary goal to recover f .)

The data misfit term should reflect the distribution of data errors. Since our data are Poisson distributed, a natural data misfit term would be the negative log-likelihood function, which is given by $\sum_{j=1}^N g(\mathbf{x}_j) - G_j \log g(\mathbf{x}_j)$. We define a piecewise constant approximation $g^\delta \in L^2(\Omega')$ of the data (G_j) and approximate the negative log-likelihood by a second order Taylor expansion at G_j . This leads to a weighted L^2 space $\mathcal{Y} := L^2(\Omega', w)$ with norm $\|g\|_{\mathcal{Y}}^2 = \int_{\Omega'} g^2(\mathbf{x})w(\mathbf{x}) d\mathbf{x}$ and weight function

$$w(\mathbf{x}) = \frac{1}{2 \max(g^\delta(\mathbf{x}), c)}, \quad \mathbf{x} \in \Omega'.$$

Here $c > 0$ is a small constant avoiding division by zero. As usually multiple weaker sources contribute to the data noise, a suitable choice of c is the background noise level. Better approximations to the Poisson log-likelihood can be achieved by taking a Taylor expansion at $g_n = F_{4\text{Pi}}(f_n, \phi_n)$ and iterating in a sequential quadratic programming manner, but for the count rates in our experimental data this did not lead to a noticeable improvement.

In summary, the precise definition of our forward operator is as follows:

$$\begin{aligned} F_{4\text{Pi}} : L^2(\Omega) \times H^2(\Omega') &\longrightarrow L^2(\Omega', w) \\ (F_{4\text{Pi}}(f, \phi))(\mathbf{x}) &:= \int_{\Omega} p(\mathbf{x} - \mathbf{y}, \phi(\mathbf{x}))f(\mathbf{y}) d\mathbf{y}, \quad \mathbf{x} \in \Omega'. \end{aligned} \quad (3.2)$$

Note that $F_{4\text{Pi}}$ does not change if $p(\cdot, \varphi)$ is replaced by its periodic extension with period cell Ω' .

Lemma 3.1. *If $p : \prod_{j=1}^3 (\mathbb{R}/(2(R_j + r_j)\mathbb{Z})) \times (\mathbb{R}/\pi\mathbb{Z}) \rightarrow \mathbb{R}$ is continuous and continuously differentiable with respect to its last argument, then the operator $F_{4\text{Pi}}$ defined in (3.2) is Fréchet differentiable on \mathcal{X} with*

$$F'_{4\text{Pi}}[f, \phi](h_f, h_\phi)(\mathbf{x}) = \int_{\Omega} \left\{ p(\mathbf{y} - \mathbf{x}, \phi(\mathbf{x}))h_f(\mathbf{y}) + \frac{\partial p}{\partial \phi}(\mathbf{y} - \mathbf{x}, \phi(\mathbf{x}))f(\mathbf{y})h_\phi(\mathbf{x}) \right\} d\mathbf{y}, \quad (3.3)$$

and the adjoint of $F'[f, \phi] : L^2(\Omega) \times H^2(\Omega) \rightarrow L^2(\Omega', w)$ is given by

$$F'_{4\text{Pi}}[f, \phi]^* g = \begin{pmatrix} \int_{\Omega'} p(\cdot - \mathbf{x}, \phi(\mathbf{x}))g(\mathbf{x})w(\mathbf{x})d\mathbf{x} \\ j^* \left(gw \int_{\Omega} \frac{\partial p}{\partial \phi}(\cdot - \mathbf{y}, \phi(\cdot))f(\mathbf{y})d\mathbf{y} \right) \end{pmatrix} \quad (3.4)$$

where $j : H^2(\Omega') \hookrightarrow L^2(\Omega')$ is the embedding operator. Moreover, $F'_{4\text{Pi}}$ satisfies the Lipschitz condition (2.3) if $\frac{\partial p}{\partial \phi}$ is uniformly Lipschitz continuous with respect to its last argument.

Proof (sketch). The Fréchet differentiability of F and eq. (3.3) follow from a Taylor expansion of the kernel p with standard estimates on the Taylor remainder and the continuity of the embedding $H^2(\Omega') \hookrightarrow L^\infty(\Omega')$. The adjoint $F'[f, \phi]^*_{L^2}$ of the continuous extension $F'[f, \phi]_{L^2}$ of $F'[f, \phi]$ to $L^2(\Omega) \times L^2(\Omega')$ can be computed by interchanging the order of integration. Then (3.4) follows from $F'[f, \phi]^* = (F'[f, \phi]_{L^2} \begin{pmatrix} 1 & 0 \\ 0 & j \end{pmatrix})^* = \begin{pmatrix} 1 & 0 \\ 0 & j^* \end{pmatrix} F'[f, \phi]^*_{L^2}$. The statement on Lipschitz continuity is straightforward. \square

The crucial observation for an efficient implementation of $F_{4\text{Pi}}$ and $F'_{4\text{Pi}}$ is that p can be separated into

$$p(z, \varphi) = \sum_{m=-M}^M \exp(im\varphi)A_m(z)$$

with $A_m \in L^2(\prod_{j=1}^3 (\mathbb{R}/(2(R_j + r_j)\mathbb{Z})))$. This was observed by Baddeley et al. in [1] for the approximation (1.4) and by Vicidomini et al. in [18] for the model (3.1). Hence,

$$(F_{4\text{Pi}}(f, \phi))(\mathbf{x}) = \sum_{m=-M}^M \exp(im\phi(\mathbf{x})) \int_{\Omega'} A_m(\mathbf{x} - \mathbf{y})f(\mathbf{y}) d\mathbf{y}, \quad \mathbf{x} \in \Omega'.$$

Here f is extended by 0 in $\Omega' \setminus \Omega$ (zero-padding). The convolution integrals can be evaluated efficiently using FFT. An analogous procedure can be applied for the evaluation of $F'[f, \phi]$ and its adjoint.

We approximated the phase ϕ using tensor products of Chebychev polynomials, for which the Gramian matrix with respect to the H^2 inner product can be computed explicitly.

3.2 Implementation and necessity of the nonnegativity constraint

We solve the constrained quadratic minimization problems

$$(f_{n+1}, \phi_{n+1}) := \operatorname{argmin}_{\substack{(f, \phi) \in L^2(\Omega) \times H^2(\Omega), \\ f \geq 0 \text{ a.e.}}} \|F'_{4\text{Pi}}[(f_n, \phi_n)](f, \phi) - g_n\|^2 + \alpha_n \|(f, \phi) - (f_0, \phi_0)\|^2, \quad (3.5)$$

with

$$g_n := F'_{4\text{Pi}}(f_n, \phi_n) - F_{4\text{Pi}}((f_n, \phi_n)) + g_\delta$$

using the semi-smooth Newton method (cf. [11]). In each step of this method an unconstrained, positive definite linear system has to be solved, which is done by the conjugate gradient method. In Figure 3.1 the reconstruction of a fluorophore density and the phase from a 2d-slice of real 4Pi data is shown. To

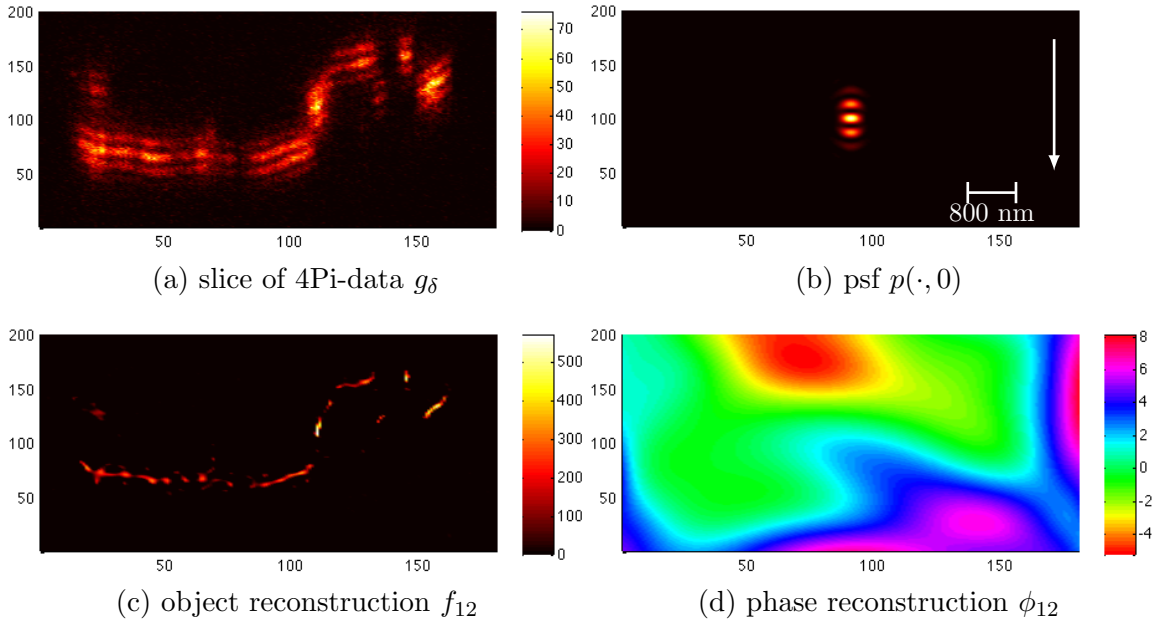


Figure 3.1: Panel (a) shows a slice of real 3-dimensional 4Pi-data, where in the approximate center the waves were interfering destructively. From these data the reconstructions of object (c) and phase (d) have been obtained with the constrained IRGNM for $f_0 = 0$ and $\phi_0 = 0$. The reconstruction of the phase reflects the constructive interference on the left and right side of the data and the destructive interference in the center. The modeled psf (for constructive interference) is depicted in panel (b) together with indications on the scale and the optical axis (represented by the arrow). To reconstruct the phase we used a basis of polynomials with maximal degree 7 in each dimension.

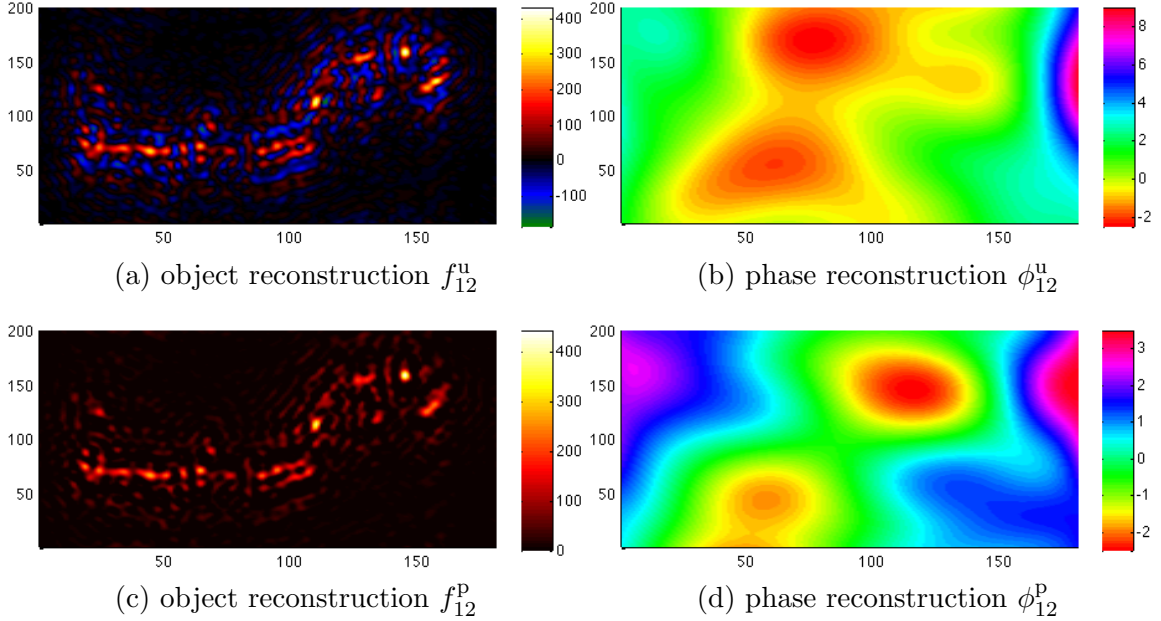


Figure 3.2: Panels (a) and (b) show reconstructions of object and phase respectively from the data shown in Figure 3.1a, which have been obtained by the unconstrained IRGNM. The phase is very badly reconstructed which leads to remaining sidelobes in the object reconstruction. This is most eminent in the center where the psf features destructive interference. The same deficiencies can be observed in panels (c) and (d), where the nonnegativity constraint has been incorporated by a simple projection after each step. All of the reconstructions depicted in Figures 3.1 and 3.2 were performed with the same regularization parameters.

demonstrate the necessity to incorporate nonnegativity constraint into the minimization problem, in Figure 3.2 we display reconstructions from the same data, without constraint and with simply projecting onto \mathcal{C} after an unconstrained IRGNM step, i.e. for the iteration schemes

$$(f_{n+1}^u, \phi_{n+1}^u) := \operatorname{argmin}_{(f, \phi) \in L^2(\Omega) \times H^2(\Omega)} \left[\|F'_{4\text{Pi}}[(f_n^u, \phi_n^u)](f, \phi) - g_n\|^2 + \alpha_n \|(f, \phi) - (f_0, \phi_0)\|^2 \right],$$

$$(f_{n+1}^p, \phi_{n+1}^p) := P_{\mathcal{C}} \operatorname{argmin}_{(f, \phi) \in L^2(\Omega) \times H^2(\Omega)} \left[\|F'_{4\text{Pi}}[(f_n^p, \phi_n^p)](f, \phi) - g_n\|^2 + \alpha_n \|(f, \phi) - (f_0, \phi_0)\|^2 \right].$$

Here the metric projection is given by $P_{\mathcal{C}}(f, \phi) = (\max(f, 0), \phi)$. Comparing the reconstructions of Figures 3.1 and 3.2 it is obvious that the incorporation of the nonnegativity constraint in the minimization problem is necessary for accurate reconstructions of the phase.

A further option pursued in [18] is to update f and ϕ in alternating manner such that in each update step for f a constrained minimization problem for f only instead of both f and ϕ has to be solved. However, such a procedure requires significantly more iteration steps.

3.3 Results for simulated and experimental data

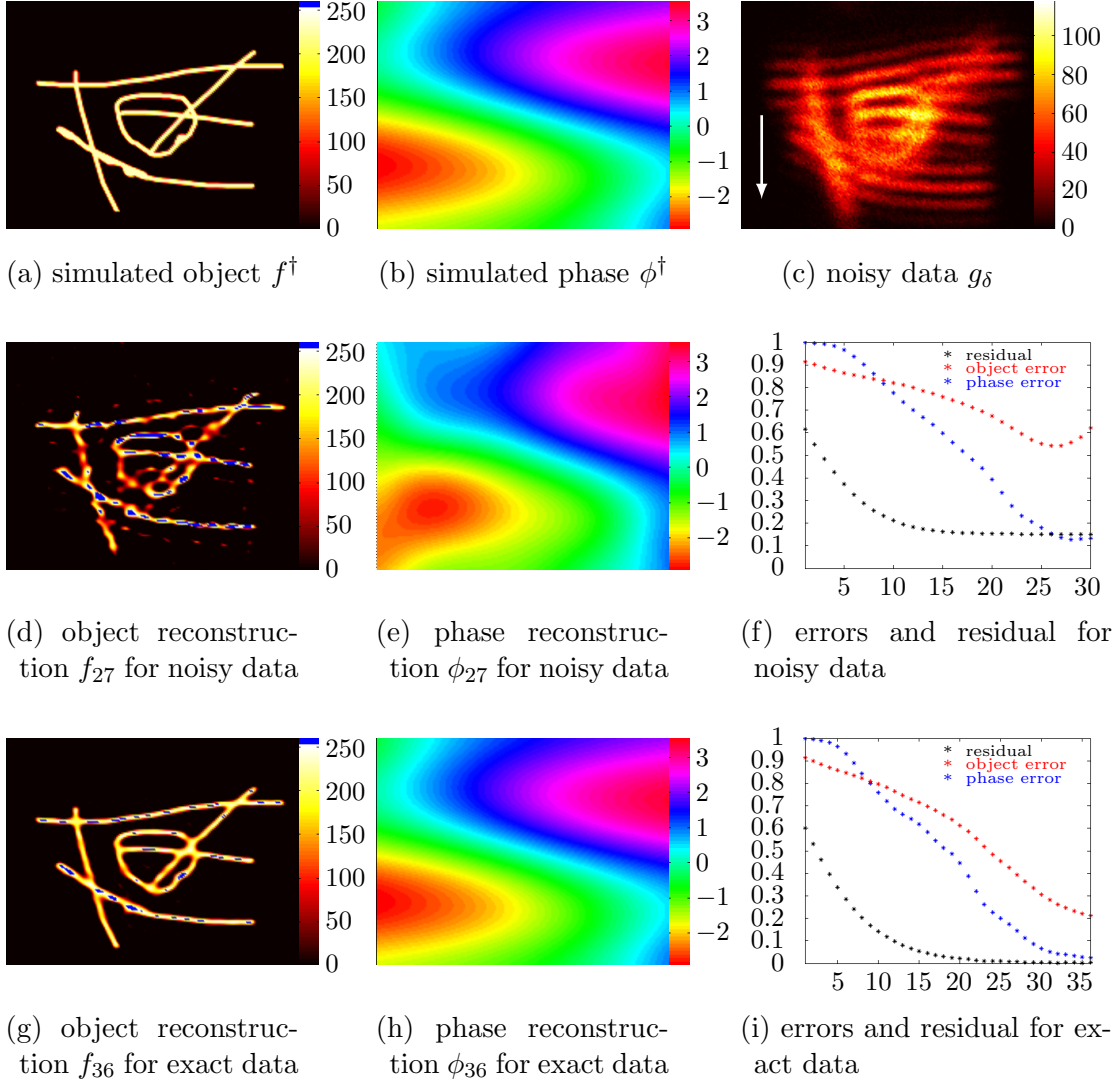


Figure 3.3: Panels (a) and (b) show a simulated object and phase, and panel (c) the corresponding 4Pi-data perturbed with Poisson-noise. Panels (d) and (e) show the reconstructions of object and phase respectively from this noisy data obtained with the constrained IRGNM. In panel (f) the residual $\|g_\delta - F(f_n, \phi_n)\|_{L^2}$, the object error $\|f_n - f^\dagger\|_{L^2}$, and the phase error $\|\phi_n - \phi^\dagger\|_{L^2}$ are plotted over the iteration index n . Panels (g)–(i) are analogous to panels (d)–(f) with noisy data g_δ replaced by exact data $F(f^\dagger, \phi^\dagger)$.

Figure 3.3 shows reconstructions from simulated two-dimensional noisy and exact data. Here we chose polynomials of maximal degree 7 in each dimension to approximate the reconstructed phase. We chose the exact phase as a shifted sum of a sine and arctan function, which does not belong to the polynomial subspace.

For exact data the sidelobes are removed completely, and for noisy data at the given count rate only very little of the sidelobes is left in the reconstruction. The required number of semi-smooth Newton (SSN) steps increases with n . To give an idea, we mention that less than 8 SSN steps were needed for $n \leq 21$ with less than 80 CG steps in each SSN step, and for $n = 30$ the algorithm required 49 SSN steps with less than 600 CG steps. We must say that the stopping indices for the Gauß-Newton iteration are chosen somewhat arbitrarily in this paper. The development of a good stopping rule for the kind of errors considered in this paper, nonlinear operators and convex constraints is an interesting topic for future research.

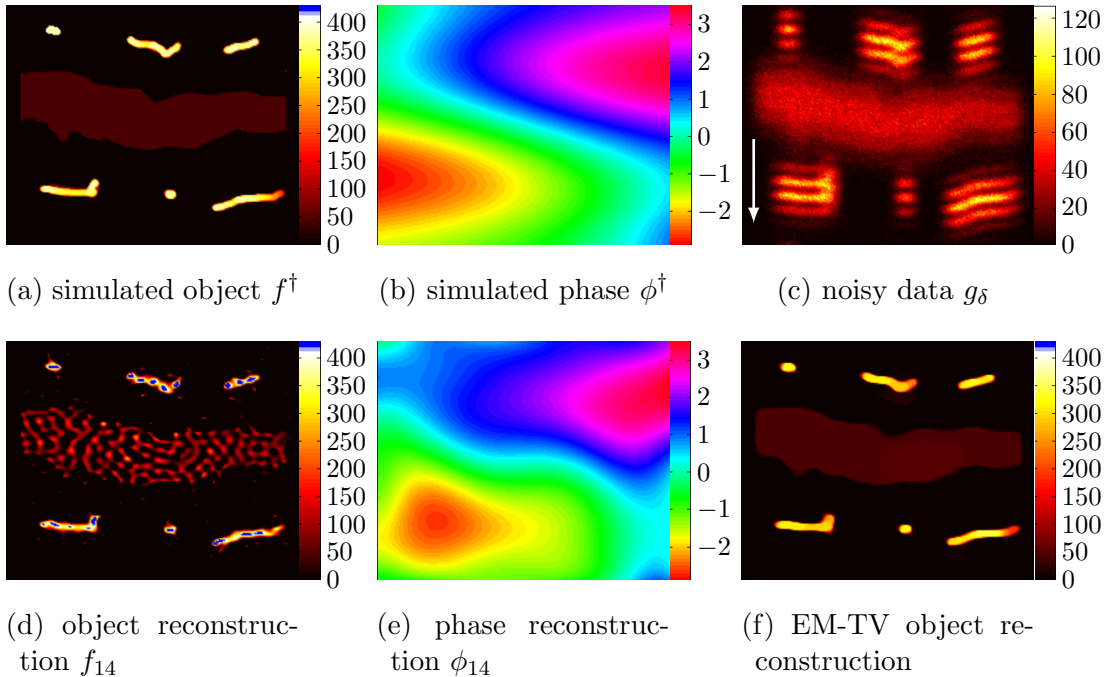


Figure 3.4: Panels (a) and (b) show a simulated object and phase from which noisy 4Pi data was created (panel (c)). Panel (d) depicts the object reconstruction obtained with the IRGNM and panel (e) the corresponding phase reconstruction. Panel (f) shows a reconstruction by an expectation maximization algorithm with TV penalty using the reconstructed phase (e).

In Figure 3.4 we chose an object which is constant in a region, and hence the data carry no information on the phase there. Due to the H^2 -phase penalty term, the phase is interpolated smoothly in this area and recovered quite well, except in dark areas close to the boundary. In contrast, the reconstruction of the object exhibits a grainy structure in the central area. This is a consequence of choosing the L^2 norm as object penalty. Since we have found a good approximation ϕ_{app} of the phase, we can compute a better reconstruction of the object in a second step by solving an inverse problem for the linear operator $f \mapsto F(f, \phi_{\text{app}})$. The

result in Figure 3.4e was computed using an expectation-maximization method with a TV penalty term and Bregman iterations as described in [5].

Figure 3.5 shows cuts through 3-dimensional experimental data. The corresponding reconstructions of object and phase are shown in Figure 3.6. Note that due to the simultaneous reconstruction of the phase function the non-symmetric sidelobes in the data have been removed in the object reconstruction. Including

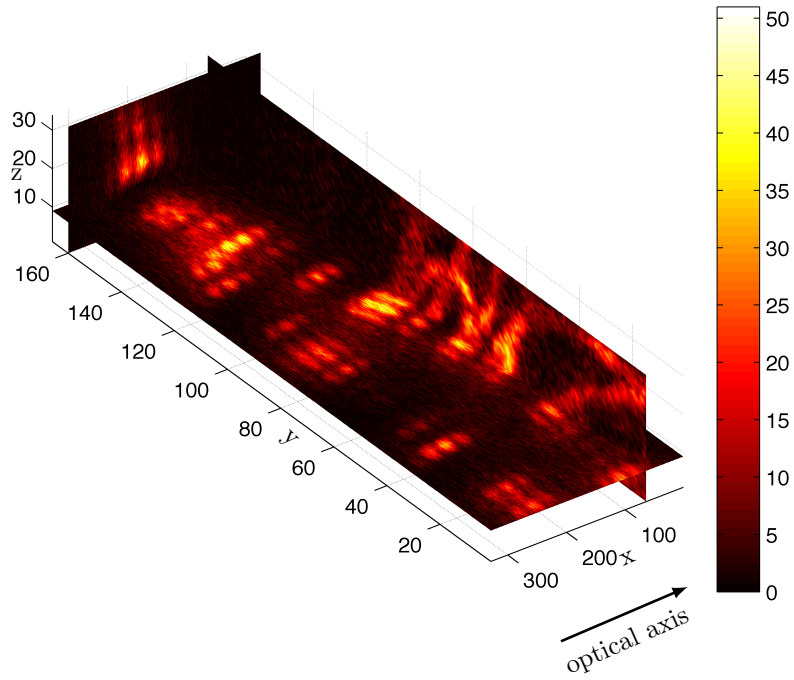


Figure 3.5: Data of microtubules in a Vero cell, for $NA = 1.34$, $\lambda_{\text{ex}} = 635\text{nm}$, $\lambda_{\text{em}} = 680\text{nm}$. The data extension is $(2952\text{nm} \times 9296\text{nm} \times 1904\text{nm})$ in x , y and z direction respectively. The annotations at the axes number the voxels in the respective dimension.

the zero padding, the data contained approximately 2 million voxels. The phase has been approximated by Chebychev polynomials of maximal degree 3 in each dimension.

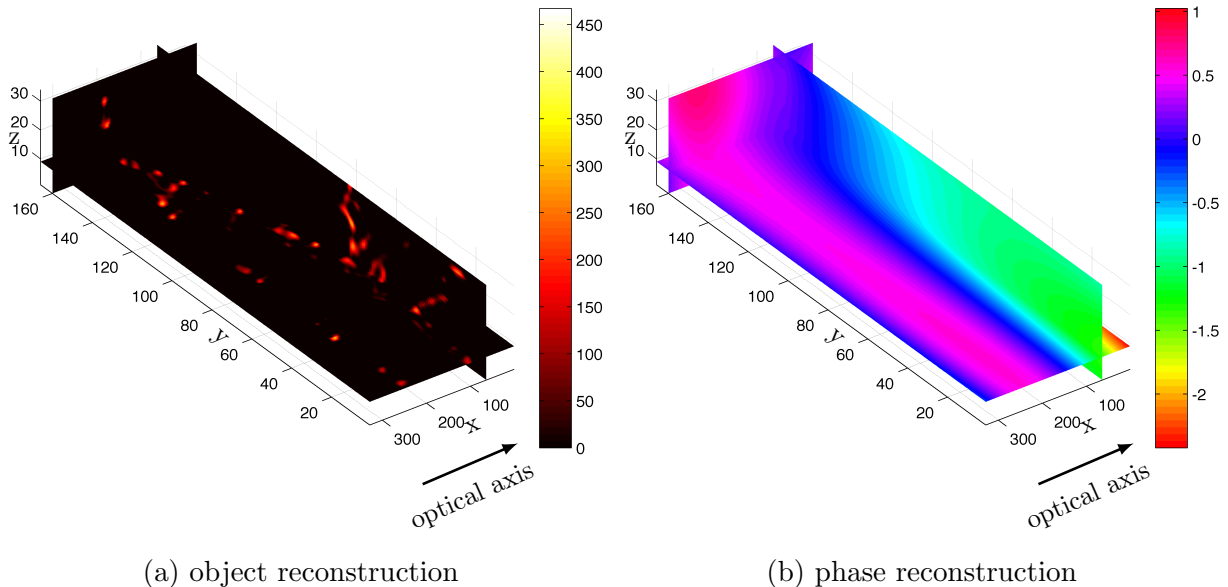


Figure 3.6: Panel (a) shows the reconstruction of the object from the data shown in Figure 3.5. In Panel (b) the corresponding reconstruction of the phase is depicted.

Acknowledgments

We would like thank Andreas Schönle and Giuseppe Vicidomini (MPI biophysical chemistry, Göttingen) for their support concerning microscopic data and information on 4Pi-microscopy. We further thank Jan Keller for his matlab code implementing the 4Pi-psf model (3.1). Finally, we gratefully acknowledge financial support by BMBF (German Federal Ministry for Education and Science) under the project INVERS.

References

- [1] D. Baddeley, C. Carl, and C. Cremer. 4Pi microscopy deconvolution with a variable point-spread function. *Applied Optics*, 45(27):7056 – 7064, 2006.
- [2] A. B. Bakushinskii. The problem of the convergence of the iteratively regularized Gauß-Newton method. *Comput. Maths Math. Phys.*, 32(9):1353–1359, 1992.
- [3] A. B. Bakushinskiĭ and M. Y. Kokurin. *Iterative Methods for Approximate Solution of Inverse Problems*. Springer, Dordrecht, 2004.
- [4] B. Blaschke, A. Neubauer, and O. Scherzer. On convergence rates for the iteratively regularized Gauß-Newton method. *Journal of Numerical Analysis*, 17:421–436, 1997.

- [5] C. Brune, A. Sawatzky, and M. Burger. Bregman-EM-TV methods with application to optical nanoscopy. In X.-C. Tai et al., editors, *Proceedings of the 2nd International Conference on Scale Space and Variational Methods in Computer Vision*, volume 5567, page 235. Springer LNCS, 2009.
- [6] H. W. Engl, M. Hanke, and A. Neubauer. *Regularization of Inverse Problems*. Kluwer Academic Publishers, 1996.
- [7] L. C. Evans. *Partial differential equations*. Graduate Studies in Mathematics 19. AMS, Providence, RI, 1998.
- [8] H. Harbrecht and T. Hohage. A newton method for reconstructing non star-shaped domains in electrical impedance tomography. *Inverse Problems and Imaging*, 3:353–371, 2009.
- [9] S. Hell and E. H. K. Stelzer. Fundamental improvement of resolution with a 4Pi-confocal fluorescence microscope using two-photon excitation. *Optics Communications*, 93:277–282, 1992.
- [10] S. Hell and E. H. K. Stelzer. Properties of a 4Pi confocal fluorescence microscope. *J. Opt. Soc. Am. A*, 9(12):2159 – 2166, December 1992.
- [11] M. Hintermüller, K. Ito, and K. Kunisch. The primal-dual active set strategy as a semismooth Newton method. *SIAM J. OPTIM.*, 13(3):865–888, 2003.
- [12] T. Hohage. Logarithmic convergence rates of the iteratively regularized Gauss-Newton method for an inverse potential and an inverse scattering problem. *Inverse Problems*, 13:1279–1299, 1997.
- [13] T. Hohage. Regularization of exponentially ill-posed problems. *Numer. Funct. Anal. Optim.*, 21:439–464, 2000.
- [14] B. Kaltenbacher and B. Hofmann. Convergence rates for the iteratively regularized Gauss-Newton method in Banach spaces. *Inverse Problems*, 26:035007, 2010.
- [15] B. Kaltenbacher, A. Neubauer, and O. Scherzer. *Iterative Regularization Methods for Nonlinear ill-posed Problems*. Radon Series on Computational and Applied Mathematics. de Gruyter, Berlin, 2008.
- [16] A. Neubauer. Tikhonov-regularization of ill-posed linear operator equations on closed convex sets. *Journal of Approximation Theory*, 53:304–320, 1988.
- [17] J. B. Pawley, editor. *Handbook of Biological and Confocal Microscopy*. Plenum Press, New York, 2 edition, 1995.
- [18] G. R. S. Vicidomini, A. Egner, S. W. Hell, and A. Schönle. Automatic deconvolution in 4Pi-microscopy with variable phase. *Opt. Exp.*, 18(8):10154 – 10167, 2010.